Angewandte Zuschriften

Enzyme Specificity

DOI: 10.1002/ange.201400220

Structural Basis of Chitin Oligosaccharide Deacetylation**

Eduardo Andrés, David Albesa-Jové, Xevi Biarnés, Bruno M. Moerschbacher, Marcelo E. Guerin, and Antoni Planas**

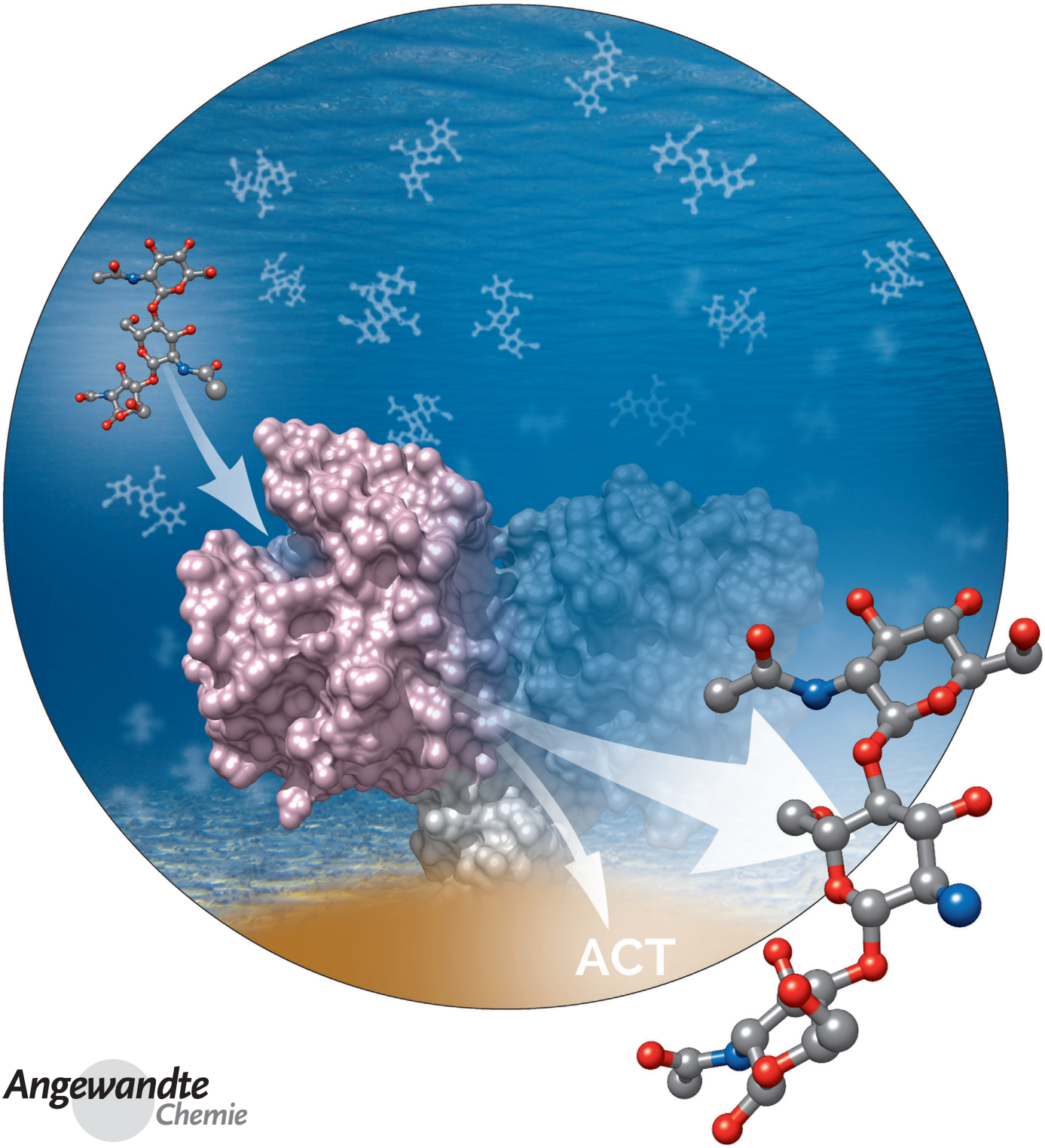

Abstract: *Cell signaling and other biological activities of chitooligosaccharides (COSs) seem to be dependent not only on the degree of polymerization, but markedly on the specific de-N-acetylation pattern. Chitin de-N-acetylases (CDAs) catalyze the hydrolysis of the acetamido group in GlcNAc residues of chitin, chitosan, and COS. A major challenge is to understand how CDAs specifically define the distribution of GlcNAc and $GlcNH_2$ moieties in the oligomeric chain. We report the crystal structure of the Vibrio cholerae CDA in four relevant states of its catalytic cycle. The two enzyme complexes with chitobiose and chitotriose represent the first 3D structures of a CDA with its natural substrates in a productive mode for catalysis, thereby unraveling an induced-fit mechanism with a significant conformational change of a loop closing the active site. We propose that the deacetylation pattern exhibited by different CDAs is governed by critical loops that shape and differentially block accessible subsites in the binding cleft of CE4 enzymes.*

Chitin, the linear polysaccharide of β-(1-4)-linked *N*-acetylglucosamine (GlcNAc) units, represents the second most abundant natural polymer on earth after cellulose.[1] Chitin processing, mainly in the form of depolymerization and de-N-acetylation reactions, generates a series of derivatives including chitosan and chitooligosaccharides (COSs), which play remarkable roles in nature.[2–5] COSs are particularly apparent in molecular recognition events, including the modulation of cell signaling and morphogenesis, the immune response, and host–pathogen interactions. One of the most striking examples that highlight the importance of COSs is represented by the Nod factors, key signal molecules produced by rhizobia that initiate the development of root nodules in leguminous host plants.[6,7] Most of the biological activities associated with COSs seem to be largely dependent on the degree of polymerization and the specific de-N-acetylation pattern, which define the charge density and the distribution of GlcNAc and $GlcNH_2$ moieties in chitosan and COS.[8,9]

Chitin de-N-acetylases (CDAs) catalyze the hydrolysis of the acetamido group in *N*-acetylglucosaminyl residues of chitin, chitosan, and COSs.[2,10,11] CDAs belong to family 4 of carbohydrate esterases, which also comprises acetylxylan esterases and peptidoglycan deacetylases (CE4).[12] CDAs are found to be widely distributed in fungi, not only as intracellular (periplasmic) CDAs involved in fungal cell wall formation, sporulation, and in the catabolism of COSs, but also as extracellular enzymes to modify the cell-wall chitin.[10,13] Plant fungal pathogens such as *Colletotrichum lindemuthianum* secrete CDAs during infection and initial growth phase in the host, which partially deacetylate the exposed fungal cell-wall chitin polymers, thus preventing the action of host plant chitinases that trigger the plant defense system.[5] More recently, a similar strategy has also been suggested for human pathogenic fungi.[14] CDAs are also found in some insects,[15] and in marine bacteria of the *Vibrionaceae* family, widely distributed in oceans and mainly responsible for recycling nitrogen present in chitinous debris.[16] CDAs are current targets for the design of antifungal and antibacterials in biofilm formation, and for biotechnological production of partially deacetylated COSs with applications in medicine and plant protection.[10,11,17]

The deacetylation pattern exhibited by CDAs and related CE4 enzymes active on COSs is diverse, some being specific for a single position (e.g. *Rhizobium* NodB[18] and *V. cholerae*[19]), others showing multiple attack (e.g. *C. lindemuthianum* CDA[20,21]). A major challenge is to understand how these enzymes define the distribution of GlcNAc and $GlcNH_2$ moieties in the oligomeric chain. To advance on the comprehension of the molecular mechanism that governs CDA substrate binding and specificity we performed detailed structural and biochemical analysis of the chitin de-N-acetylase *Vc*CDA from the human pathogen *V. cholerae*, which de-N-acetylates the penultimate GlcNAc moiety from the nonreducing end of short-length COSs[19] and is part of a complex chitin degradation pathway.[19,22,23] To this end, *Vc*CDA was expressed in *E. coli* as the full-length protein without the signal peptide (first 26 amino acids) and with a Strep-tag at the C-terminus. The recombinant enzyme purified as the monomeric form in solution was active on $(GlcNAc)_{n=2-4}$ substrates, with an optimum pH value between 8 and 9 (see Figure S3 in the Supporting Information). Kinetics with chitobiose ($n=2$) showed cooperative behavior, with a Hill index $h=1.92$. The larger COSs ($n=3,4$) showed Michaelis–Menten kinetics, with 8 and 24-fold lower k_{cat} values than chitobiose (Figure 1a). The disaccharide DP2 proved to be the best substrate, in agreement with previous reports on *Vc*CDA.[19]

The crystal structures of *Vc*CDA in three relevant states of its catalytic cycle, including the ligand-free and complexed forms with GlcNAc (DP1) and $(GlcNAc)_2$ (DP2), were determined (see Table S1 in the Supporting Information). *Vc*CDA is organized in three distinct domains: the N-terminal

[*] Dr. E. Andrés,[+] Dr. X. Biarnés, Prof. A. Planas
Laboratory of Biochemistry, Institut Químic de Sarrià
Universitat Ramon Llull
Via Augusta 390, 08017 Barcelona (Spain)
E-mail: antoni.planas@iqs.edu
Dr. D. Albesa-Jové,[+] Prof. M. E. Guerin
Unidad de Biofísica, Consejo Superior de Investigaciones Científicas—Universidad del País Vasco/Euskal Herriko Unibertsitatea (CSIC-UPV/EHU) and Departamento de Bioquímica
Universidad del País Vasco
48940 Leioa, Bizkaia (Spain)
Prof. M. E. Guerin
IKERBASQUE
48011 Bilbao (Spain)
E-mail: mrcguerin@gmail.com
Prof. B. M. Moerschbacher
Institut für Biologie und Biotechnologie der Pflanzen, Universität Münster (Germany)
[+] These authors contributed equally to this work.

[**] This work was supported by the European Commission ERA-IB PIM2010EEI-0072 (to A.P.) and HEALTH-F3-2011-260872, SAF2010-19096, and IKERBASQUE (to M.E.G.). We gratefully acknowledge ESRF, DLS, and SLS for granting access to synchrotron radiation facilities. D.A.-J. acknowledges the support from Fundación Biofísica Bizkaia. We acknowledge Hugo Aragunde (IQS) for kinetic experiments.

Supporting information for this article is available on the WWW under http://dx.doi.org/10.1002/anie.201400220.

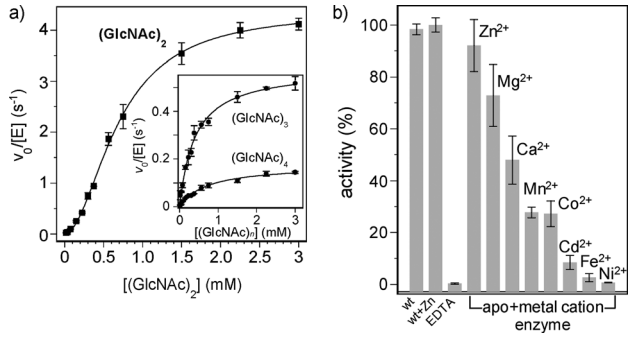

Figure 1. a) VcCDA kinetics with $(GlcNAc)_n$ ($n=2$–4) substrates in 50 mM phosphate buffer at pH 8.5, 300 mM NaCl, 37 °C. Kinetic parameters: $(GlcNAc)_2$, $k_{cat}=4.38\pm0.08\ s^{-1}$, $K_M=0.69\pm0.02$ mM, $h=1.92$; $(GlcNAc)_3$, $k_{cat}=0.58\pm0.02\ s^{-1}$, $K_M=0.40\pm0.03$ mM; $(GlcNAc)_4$, $k_{cat}=0.18\pm0.01\ s^{-1}$, $K_M=0.72\pm0.08$ mM. b) Relative activity with different metal cations. After treatment with ethylenediaminetetraacetic acid (EDTA) the protein was incubated with 1 mM metal cation (as the MCl_2 salt), and the activity was determined with 2 mM chitobiose as substrate.

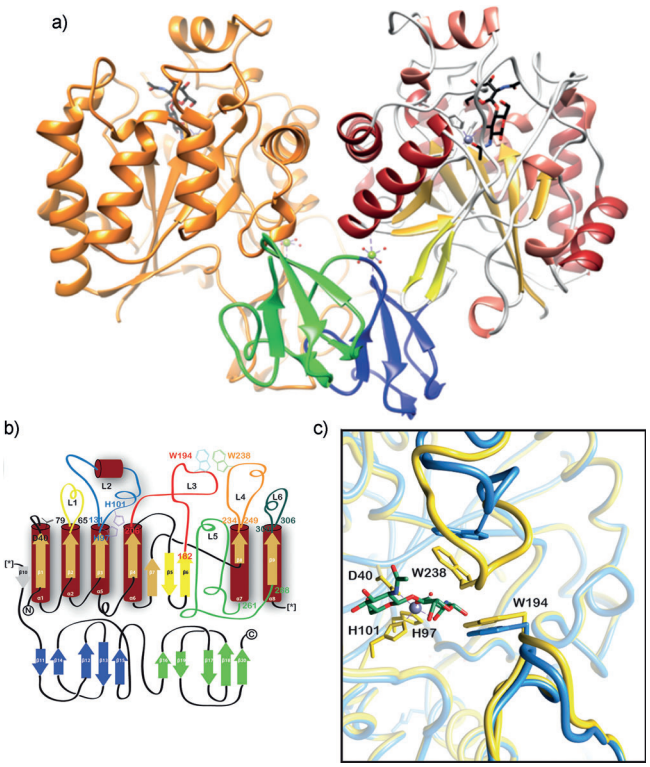

Figure 2. *Vc*CDA overall fold. a) Schematic representation showing the overall structure of the *Vc*CDA homodimer. One monomer is represented in orange, while the different domains are colored in the other monomer; the esterase domain is shown in red and yellow, while the CBMs are colored blue and green. b) Topology diagram of a *Vc*CDA monomer. The upper part shows the esterase domain, with loops 1 to 6 labeled. The lower part corresponds to the CBM1 and CBM2, shown in blue and green, respectively. c) A close-up view of the conformational changes observed in L3 and L4 between the apo enzyme (blue) and $VcCDA_{D39S}$-DP2 complex (yellow). Most significant is the structural variability of L4, which is involved in the modulation of the entrance and release of substrates.

catalytic domain (residues 27–334) corresponds to a carbohydrate esterase domain (CDA), whereas the second and third domains (residues 338–431) consist of two consecutive carbohydrate-binding modules (CBMs; Figure 2a). *Vc*CDA crystallized as a homodimer with an extensive interphase corresponding to 14–24% of the entire surface area of each monomer, and with all CDA and CBM domains participating in dimerization contacts (see the Supporting Information for details).

The carbohydrate esterase domain of *Vc*CDA adopts a $(\beta/\alpha)_7$ topology, as observed in other members of the CE4 family.[24,25] The central core comprises seven parallel β-strands that form a greatly distorted β-barrel surrounded by α-helices (Figure 2). A series of loops decorate the β-barrel and build the majority of the deeply buried carbohydrate-binding pocket, comprising residues 71–79 (loop 1; L1), 97–131 (loop 2; L2), 182–206 (loop 3; L3), 234–249 (loop 4; L4), 261–288 (loop 5; L5), and 300–306 (loop 6; L6) (Figure 2b). Three of these loops are stabilized by intramolecular disulfide bridges, including Cys106–Cys118 (loop 2), Cys185–Cys200 (loop 3), and Cys264–Cys281 (loop 5). *Vc*CDA is a metalloenzyme in which a divalent metal cation coordinates with His97, His101 (loop 2), and Asp40, a catalytic triad highly conserved among members of the CE4 family and other esterases/hydrolases.[26,27] Most of the CE4 enzymes characterized to date use predominantly Co^{2+} and Zn^{2+} ions as divalent metal cofactors in vitro.[24,25,28] As depicted in Figure 1b, kinetic studies indicate that *Vc*CDA prefers Zn^{2+} for maximal activity in vitro, with all the crystal structures reported here showing a Zn^{2+} ion in the active site.

To uncover the structural features of *Vc*CDA associated with the DP2 substrate we have produced an enzymatically inactive mutant in which Asp39 was replaced by a Ser residue. This residue is located in the "TFDD" motif, which is highly conserved among the CE4 family of enzymes, and its catalytic function has been proved by structural and mutational analysis (e.g. *S. pneumoniae* peptidoglycan deacetylase PgdA[25]). The crystal structure of the $VcCDA_{D39S}$-DP2 ($VcCDA_{D39S}$ is denoted m*Vc*CDA hereafter) complex was determined in two different crystal forms (named m*Vc*CDA-DP21 and m*Vc*CDA-DP22) at 2.1 Å resolution (see Table S1 in the Supporting Information). Two molecules of DP2 were unambiguously identified in the difference electron density maps of the m*Vc*CDA-DP22 dimer, whereas only one molecule of DP2 was found in the m*Vc*CDA-DP21 complex. DP2 binds to a deeply buried pocket in subsites −1 and 0, mostly formed by aromatic residues including Trp67, His68, His97 (catalytic triad; L2), His101 (catalytic triad, L2), His124 (L2), Trp194 (L3), Tyr169, Trp229, Trp238 (L4), His295, and Phe297, all localized in the globular core of the enzyme (Figures 2 and 3). Importantly, the reaction center is clearly visible and assembled, and presumably represents the Michaelis complex. Specifically, the carboxylate group of Asp40 and the imidazol rings of His97 and His101 are involved in Zn^{2+} coordination, which is also coordinated to the O7 atom of the *N*-acetyl group and O3 hydroxy group of the GlcNAc ring. A water molecule completes the distorted octahedral coordination to the divalent metal cation. Upon activation, this water molecule is proposed to be the nucleophile responsible for removal of the *N*-acetyl group.

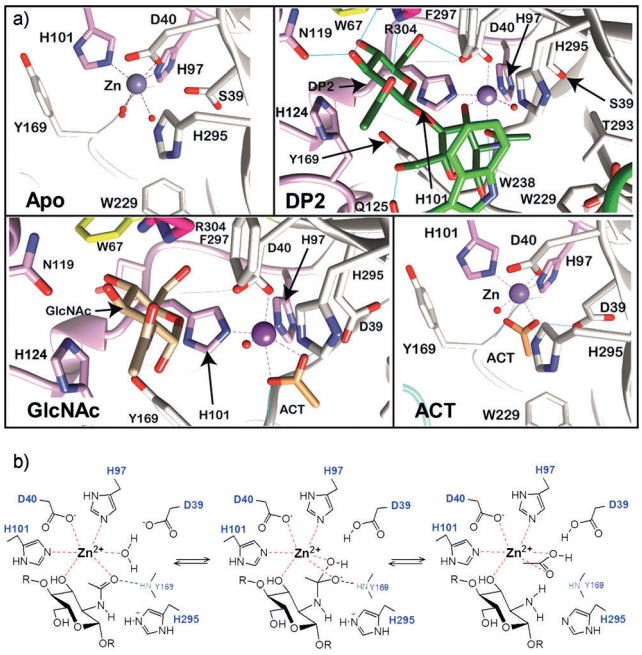

Figure 3. *Vc*CDA substrate binding specificity and catalytic mechanism. a) Closed views of the catalytic center of apo, $(GlcNAc)_2$-, GlcNAc-, and acetate-bound forms of the enzyme. b) Acid/base catalytic mechanism in *Vc*CDA involving an oxoanion intermediate stabilized by a metal cation.

Binding of the disaccharide induces significant conformational changes in the protein, as revealed by structural comparison of the three independent crystallographic monomers, in which DP2 occupies the active site, with the free *Vc*CDA monomer (Figure 2c and Figure 3a). First, the binding of DP2 to *Vc*CDA results in a major rearrangement of loop 4 towards the active site, from an "open" to a "closed" conformation (r.m.s.d. ca. 4.05 Å; Figure 2c). This structural rearrangement substantially reduces the volume of the binding cleft from about 3597 to 2789 $Å^3$. As a consequence, Trp238 stacks against the reducing end GlcNAc moiety, thereby generating a competent DP2 binding site. Secondly, the nitrogen atom Nz of the side chain amine of Lys192 (L3) forms a new hydrogen bond with the main chain of Thr121 (L2), thus allowing the Trp194 located in the same loop (L3) to close the active site. In addition, Gln125 swings its side chain into the catalytic site, thereby positioning its amide group in close contact with O5 and O6 of the sugar (Figure 3a). Molecular dynamics simulations showed that removal of DP2 from the structure results in the spontaneous opening of loop 4 at the early stages of the simulations (r.m.s.d. with respect to the "open" crystallographic conformation ca. 2.2 Å; see the Supporting Information for details).

The crystal structure of wild-type *Vc*CDA in complex with GlcNAc (*Vc*CDA-NAG) was also obtained at 1.95 Å resolution (Figure 3a; see also Table S1 in the Supporting Information). Structural comparison revealed that the GlcNAc sugar in the *Vc*CDA-NAG structure superimposes very well with the nonreducing end GlcNAc located in subsite −1 in the m*Vc*CDA-DP2 complex. There is no evidence of structural rearrangements being required to bind this particular GlcNAc unit. Subsite 0 contains a well-ordered acetate group, which is available in the mother liquor solutions and in one of the products of the de-N-acetylation reaction. It is located in the equivalent position of the acetate group of GlcNAc in subsite 0 that is observed in the m*Vc*CDA-DP2 complex, with both acetate oxygen atoms coordinating to the Zn^{2+} ion. Therefore, rearrangement of loop 4 is only triggered by the presence of a GlcNAc residue in subsite 0, as observed in the DP2 complex, thereby resulting in a productive conformation for catalysis.

CE4 esterases are proposed to operate by metal-assisted general acid/base catalysis.[24–27] To date, the crystal structure of the peptidoglycan deacetylase PdaA from *B. subtilis* (*Bs*PdaA) in complex with GlcNAc represented the only known structure of a CE4 family member solved in the presence of a sugar molecule.[29–31] Critical residues in the reaction center are preserved in *Vc*CDA/*Bs*PdaA, strongly supporting a common catalytic mechanism. However, the *Bs*PdaA complex displays a GlcNAc ligand instead of MurNAc, as it will be in the true peptidoglycan substrate of this enzyme, bound in a nonproductive conformation.[29] Thus, the m*Vc*CDA-DP2 structure represents the first relevant, likely functional, crystal structure of any de-N-acetylase in complex with substrate. Our structural data based on a competent enzyme–substrate complex allow us to delineate the two-step catalytic itinerary in *Vc*CDA, and by extension, to CE4 esterases (Figure 3b). First, a metal-bound water molecule is activated by the general base residue (Asp39) to form a tetrahedral oxyanion intermediate. The negative charge developed at the carbonyl oxygen atom is stabilized not only by metal coordination but also by the main chain nitrogen atom of Tyr169. Secondly, the nitrogen group of the intermediate is protonated by the general acid residue (His295) to assist C–N bond breaking with the generation of a free amine in the de-N-acetylated product and release of acetate.

The seven unique enzymes with their reported de-N-acetylation of *N*-acetylgluco-oligosaccharides are listed in Figure 4b Structural conservation is very high within the core (see Figure S7 in the Supporting Information). Nonetheless, there are marked differences in the loops surrounding the active site both in terms of structure and primary sequence (Figure 4b and see Figure S8 in the Supporting Information). Loop 4 is the one with the highest variability, whereas loops 2, 3, and 6 are very similar in all the structures, except for *Vc*CDA. Loops 1 and 5 are only different in *Cl*CDA and *Vc*CDA. Based on these features, we propose a "subsite-capping model" to rationalize the specific deacetylation pattern of each CDA. According to this model, these loops cap the edges of the substrate-binding cavity, thereby defining which GlcNAc unit of the oligosaccharide is placed at the catalytic site. Loops 1, 2, and 6 block the nonreducing end (negative subsites), whereas loops 3, 4, and 5 block the reducing end (positive subsites). As observed in the m*Vc*CDA-DP2 structure, chitobiose fits in the two-subsite cavity (subsites −1 and 0) defined by these loops. However, the constraints imposed by loops 4 and 5 on the reducing end (Figure 4d, middle) suggest that dynamics of these loops are required to create new positive subsites, thus allowing the enzyme to bind longer oligosaccharides (known to be

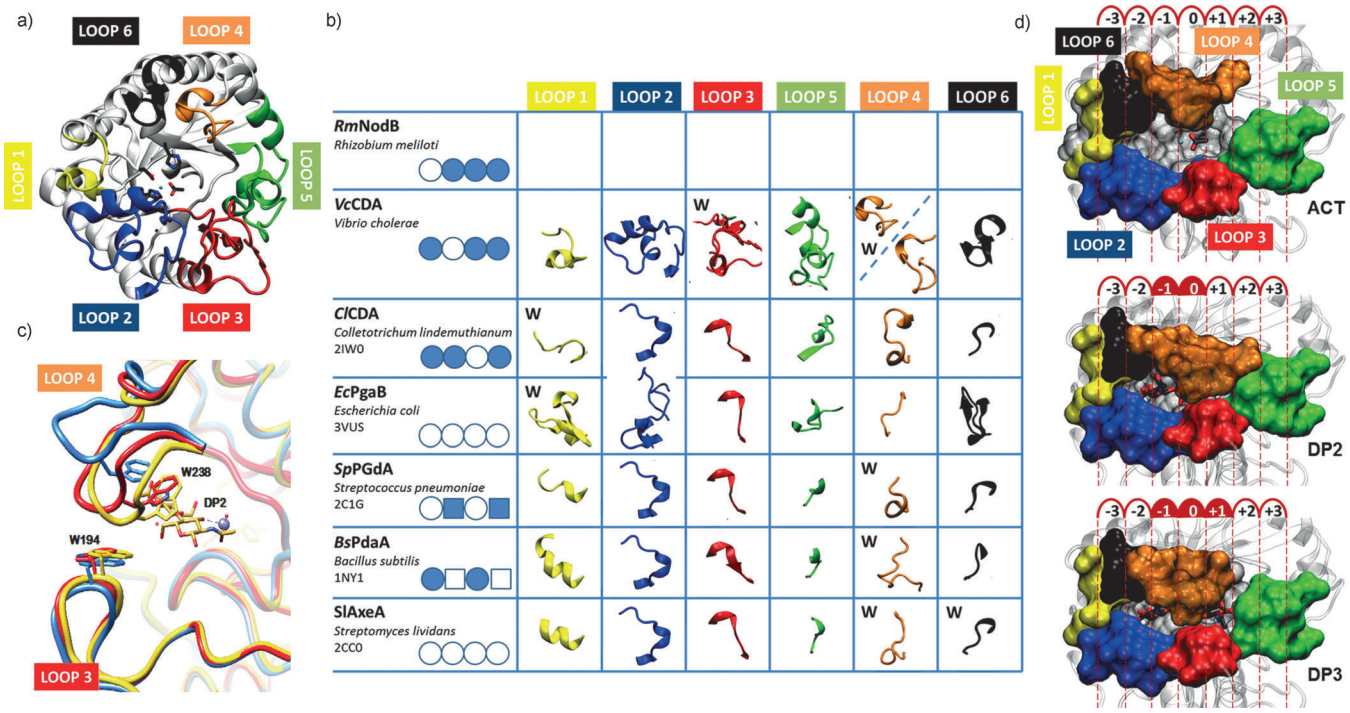

Figure 4. a) Loops surrounding the active site in *Vibrio cholerae* CDA. b) CE4 enzymes active on *N*-acetylglucosaminyl-oligosaccharides and their deacetylation pattern, comparing the loop geometries, labeled 1 to 6 as in (a). ● GlcNAc; ○ $GlcNH_2$; ■ MurNAc; □ $MurNH_2$. c) Superposition of the active site loops in *Vc*CDA in the apo form (blue), and complexes with DP2 (yellow) and DP3 (red). Only the chitobiose (DP2) substrate is shown. d) Identification of the binding subsites in *Vc*CDA. Top: the crystal structure of *Vc*CDA with acetate. Middle: the crystal structure of VcCDA in complex with chitobiose (DP2). Bottom: the crystal structure of *Vc*CDA in complex with chitotriose (DP3). The metal cation is represented as a cyan sphere in subsite 0. Substrates are represented by thick lines.

substrates, Figure 1). To test this hypothesis, we have solved the crystal structure of m*Vc*CDA in complex with a longer oligosaccharide chitotriose (DP3) at 2.2 Å resolution (see Table S1 in the Supporting Information). The GlcNAc located in the subsite −1 of DP3 fits very well in the cavity defined by loops 1, 2, and 6. Strikingly, loops 3, 4, and 5 adopt a different conformation to that observed in the unliganded and DP2 complex, thereby generating the new subsite +1 (Figure 4d). Specifically, loop 4 rearranges in a semiclosed conformation (Figure 4c), with the lateral chain of Trp238 stacking with the glycosyl residue at position +1, and lateral chains of some residues in loops 3 and 5 are displaced. Trp194 (loop 3), Trp229 (loop 4), Pro271 (loop 5), and Leu293 define the newly created hydrophobic binding pocket, which stabilizes the sugar ring. The lateral chains of Asp232 (loop 4) and Ser274 (loop 5) form two strong hydrogen bonds with O6 and O1 of this sugar moiety, respectively. The experimental m*Vc*CDA-DP3 complex support the notion that dynamics of loops 3, 4, and 5 are necessary to accommodate longer COSs in *Vc*CDA. The subsite-capping model may also apply to other CDAs with specific deacetylation patterns, such as *Cl*CDA (see the Supporting Information).

The crystal structures presented herein represent relevant states of *Vc*CDA during its catalytic cycle, supporting a metal-dependent acid/base catalytic mechanism, with the substrate directly participating in metal coordination. *Vc*CDA in its unliganded form displays the subsite −1 basically preassembled and ready to accept the DP2 substrate. In contrast, subsite 0 seems to be disassembled, with loop 4 in an open, nonproductive conformation. The binding of DP2 triggers a conformational change by closing loop 4 and generating a functionally active subsite 0. Binding of a longer oligosaccharide DP3, induces new conformational arrangements in loops 3, 4, and 5, and the opening of the subsite +1. We propose a "subsite-capping model" in which specific loops and their dynamics modulate substrate specificity and define the deacetylation pattern of CE4 enzymes. Altogether, the data reported herein might provide the bases for the rational design of CDA enzymes aimed at the biotechnological production of COSs with novel de-N-acetylation patterns for industrial and medical applications.

Received: January 8, 2014
Revised: April 2, 2014
Published online: May 8, 2014

Keywords: binding modes · bioorganic chemistry · enzyme catalysis · enzyme–substrate complexes · structure elucidation

[1] A. Varki, *Essentials of Glycobiology*, 2nd ed. (Eds.: A. Varki, R. Cummings, J. Esko, H. Freeze, P. Stanley, C. R. Bertozzi, G. Hart, M. E. Etzler), Cold Spring Harbor Laboratory Press, Cold Spring Harbor, NY, **2009**.
[2] V. Eijsink, I. Hoell, G. Vaaje-Kolstada, *Biotechnol. Genet. Eng. Rev.* **2010**, *27*, 331–366.

[3] S. B. Chavan, M. V. Deshpande, *Biotechnol. Prog.* **2013**, *23*, 10.
[4] Y. Arakane, T. Taira, T. Ohnuma, T. Fukamizo, *Curr. Drug Targets* **2012**, *13*, 442 – 470.
[5] N. E. El Gueddari, U. Rauchhaus, B. M. Moerschbacher, H. B. Deising, *New Phytol.* **2002**, *156*, 103 – 112.
[6] C. Gough, J. Cullimore, *Mol. Plant-Microbe Interact.* **2011**, *24*, 867 – 878.
[7] L. P. Hamel, N. Beaudoin, *Planta* **2010**, *232*, 787 – 806.
[8] S. K. Kim, N. Rajapakse, *Carbohydr. Polym.* **2005**, *62*, 357 – 368.
[9] N. E. El Gueddari, A. Schaaf, M. Kohlhoff, C. Gorzelanny, S. W. Schneider, B. M. Moerschbacher, *Adv. Chitin Sci.* **2007**, *10*, 119 – 126.
[10] Y. Zhao, R. D. Park, R. A. Muzzarelli, *Mar. Drugs* **2010**, *8*, 24 – 46.
[11] Y. Zhao, W. T. Ju, G. H. Jo, W. J. Jung, R. D. Park, *Biotechnol. Biopolym.* **2011**, 131 – 144.
[12] B. L. Cantarel, P. M. Coutinho, C. Rancurel, T. Bernard, V. Lombard, B. Henrissat, *Nucleic Acids Res.* **2008**, *37*, D233 – 238; http://www.cazy.org.
[13] N. M. Gilbert, L. G. Baker, C. A. Specht, J. K. Lodge, *mBio* **2012**, *3*, e00007 – 12.
[14] J. E. Urch, R. Hurtado-Guerrero, D. Brosson, Z. Liu, V. G. Eijsink, C. Texier, D. M. van Aalten, *Protein Sci.* **2009**, *18*, 1197 – 1209.
[15] S. Luschnig, T. Batz, K. Armbruster, M. A. Krasnow, *Curr. Biol.* **2006**, *16*, 186 – 194.
[16] M. J. L. Ferguson, G. W. Gooday in *Chitin enzymology* (Ed.: R. A. A. Muzzarelli), Atec, Grottammare, Italy, **1996**, pp. 393 – 396.
[17] B. K. Park, M. M. Kim, *Int. J. Mol. Sci.* **2010**, *11*, 5152 – 5164.
[18] M. John, H. Röhrig, J. Schmidt, U. Wieneke, J. Schell, *Proc. Natl. Acad. Sci. USA* **1993**, *90*, 625 – 629.
[19] X. Li, L. X. Wang, X. Wang, S. Roseman, *Glycobiology* **2007**, *17*, 1377 – 1387.
[20] K. Tokuyasu, M. Mitsutomi, I. Yamaguchi, K. Hayashi, Y. Mori, *Biochemistry* **2000**, *39*, 8837 – 8843.
[21] O. Hekmat, K. Tokuyasu, S. G. Withers, *Biochem. J.* **2003**, *374*, 369 – 380.
[22] X. Li, S. Roseman, *Proc. Natl. Acad. Sci. USA* **2004**, *101*, 627 – 631.
[23] K. L. Meibom, X. B. Li, A. T. Nielsen, C. Y. Wu, S. Roseman, G. K. Schoolnik, *Proc. Natl. Acad. Sci. USA* **2004**, *101*, 2524 – 2529.
[24] E. J. Taylor, T. M. Gloster, J. P. Turkenburg, F. Vincent, A. M. Brzozowski, C. Dupont, F. Shareck, M. S. Centeno, J. A. Prates, V. Puchart, L. M. Ferreira, C. M. Fontes, P. Biely, G. J. Davies, *J. Biol. Chem.* **2006**, *281*, 10968 – 10975.
[25] D. E. Blair, A. W. Schuttelkopf, J. I. MacRae, D. M. van Aalten, *Proc. Natl. Acad. Sci. USA* **2005**, *102*, 15429 – 15434.
[26] M. Hernick, C. A. Fierke, *Arch. Biochem. Biophys.* **2005**, *433*, 71 – 84.
[27] D. E. Blair, O. Hekmat, A. W. Schuttelkopf, B. Shrestha, K. Tokuyasu, S. G. Withers, D. M. van Aalten, *Biochemistry* **2006**, *45*, 9416 – 9426.
[28] D. J. Little, J. Poloczek, J. C. Whitney, H. Robinson, M. Nitz, P. L. Howell, *J. Biol. Chem.* **2012**, *287*, 31126 – 31137.
[29] D. E. Blair, D. M. van Aalten, *FEBS Lett.* **2004**, *570*, 13 – 19.
[30] W. Vollmer, A. Tomasz, *J. Biol. Chem.* **2000**, *275*, 20496 – 20501.
[31] T. Fukushima, H. Yamamoto, A. Atrih, S. J. Foster, J. Sekiguchi, *J. Bacteriol.* **2002**, *184*, 6007 – 6015.

